P2.2 AN ENSEMBLE-BASED 4DVAR APPROACH WITH SVD TECHNIQUE

Chongjian Qiu* and Aimei Shao
College of Atmospheric Sciences, Lanzhou University, China
Qin Xu
NOAA/National Severe Storms Laboratory, Norman, Oklahoma, USA
Li Wei
Cooperative Institute for Mesoscale Meteorological Studies, University of Oklahoma, Norman, Oklahoma, USA

1. INTRODUCTION

Four-dimensional variational (4DVar) and ensemble Kalman filter (EnKF) are two kinds of advanced data assimilation techniques. Lorenc (2003) reviewed EnKF in comparison with 4DVar, and suggested that a hybrid method may be attractive for mesoscale NWP systems. Previously, a hybrid EnKF-3DVar scheme was proposed by Hamill and Snyder (2000). Recently, a more sophisticated hybrid approach that combines EnKF and 3DVar, called maximum likelihood ensemble filter, was elaborated by Zupanski (2005). Inspired by these previous studies, this study is intended to develop a new ensemble-based hybrid approach that is relatively simple and yet practically effective in reducing problems caused by model bias errors.

The hybrid approach considered in this paper is an ensemble-based 4DVar, called En4DVar. This approach extracts the leading singular vectors from an ensemble of 4D perturbation solutions produced by the model, and then a linear combination of the extracted singular vectors is used to fit 4D innovation (observation minus background) data and thus to produce an incremental analysis in each assimilation cycle. The involved least-squares fitting is similar to that in 4DVar, but the leading singular vectors are used in place of the Green's functions (or represented solutions), so the fitting is computationally much more efficient than that in 4DVar. In the costfunction used for the fitting, the background error covariance matrix is constructed implicitly by the perturbation solutions (through their representative singular vectors). This is somewhat similar to that in EnKF, but the perturbation solutions are not updated through analysis into the next cycle so that the analysis is simpler and much more efficient than in EnKF. The potential merits of the method are demonstrated by three sets of observing system simulation experiments performed with a shallow-water equation model.

2. THE METHOD

In En4DVar the analysis increment, $\Delta\mathbf{u}_a$, is a 4D vector in a time window and is obtained through the minimization of the following cost function

$$J = \boldsymbol{ß}^T\boldsymbol{ß} + [\mathbf{H}\Delta\mathbf{u}_a - \Delta\mathbf{y}]^T\,\mathbf{O}^{-1}[\mathbf{H}\Delta\mathbf{u}_a - \Delta\mathbf{y}] \quad (1)$$

where $\mathbf{H}$ denotes the observation operator，$\Delta\mathbf{y} = \mathbf{y} - \mathbf{H}\mathbf{u}_b$ is the observation innovation with respect to the background field $\mathbf{u}_b$ at the each time level in a time window， $\mathbf{y}$ is the observation, $\mathbf{O}$ is the observation error covariance matrix, and the analysis increment with respect to the background field，$\triangle\mathbf{u}_a$，is expressed by a truncated expansion of the singular vectors to the *p*-th order, that is,

$$\Delta\mathbf{u}_a = \sum_{k=1}^{p} \mathbf{b}_k ß_k = \mathbf{B}\boldsymbol{ß} \quad (2)$$

where $\boldsymbol{ß} = (ß_1, ß_2, \ldots ß_p)^T$ is the vector composed of the coefficients (that is, the control variables for the minimization) and $\mathbf{B} = (\mathbf{b}_1, \mathbf{b}_2, \ldots \mathbf{b}_p)$ is orthogonal matrices composed of the leading *p* right singular vectors of a matrices **A.** Each data field (that is, a column vector in **A**) is given by a difference field sampled from perturbed model integration (with respect to the background run) on a 4D grid over the analysis time window centered at the ending time of the current assimilation cycle. The background integration is initialized from the starting time of the current assimilation cycle (which is also the ending time of the previous data assimilation cycle) without perturbing the initial condition, while the perturbed integration is initialized with a random perturbation field added to the initial condition. For simplicity, we assume that the analysis grid has the same N_t time levels as the observations.

Denote by τ the length of the analysis time window and by *T* the time length of each data assimilation cycle. The analysis time window for the *n*-th cycle is then between $nT - \tau/2 \le t \le nT + \tau/2$. By using the formulations in (1)-(2), the analysis can be performed over the analysis time window centered at the ending time of each assimilation cycle through the following three steps:

I. Integrate the model by using the initial condition provided by the analysis at the ending time of the previous cycle to produce the background field over the analysis time window centered at the ending time of the current assimilation cycle.

* *Corresponding author address*: Chongjian Qiu, college of Atmospheric Sciences, Lanzhou University, China. e-mail: qiucj@lzu.edu.cn

Generate M random perturbation fields by using the Monte Carlo method, and filter short wave noises spatially between neighbored grid points from these random fields. Add each filtered field to the initial condition and integrate the model to produce a perturbed 4D field over the analysis time window. Obtain M difference fields by subtracting the background field from each of the M perturbed field. Rescale the difference fields based on the estimated background error standard deviations, and perform the SVD to extract the singular vectors from the M rescaled difference fields.

II. Select the first p singular vectors so that the cumulative sum of relative energies $\sum_{k=1}^{p} E_k$ reaches a threshold value of 0.95. Use the selected first p basis vectors for the truncated expressions of the analysis increment field in (2). Use the least-squares method to compute the coefficients ß$_k$ that minimize the cost-function in (1).

III. Substitute the computed coefficients into (2) to obtain the analysis increment field and then add it with the background field to obtain the analysis field.

3. PREDICTION MODEL AND EXPERIMENT SETUP

3.1. Shallow-water Equation Model

To test the proposed method, observing system simulation experiments (OSSEs) are designed with a two-dimensional shallow-water equation model. The shallow water equations are formulated in the f-plane by

$$\partial u/\partial t = -u\partial u/\partial x - v\partial u/\partial y + fv - g\partial h/\partial x \quad (3a)$$

$$\partial v/\partial t = -u\partial v/\partial x - v\partial v/\partial y - fu - g\partial h/\partial y \quad (3b)$$

$$\partial h/\partial t = -u\partial(h - h_s)/\partial x - v\partial(h - h_s)/\partial y - (H + h - h_s)(\partial u/\partial x + \partial v/\partial y) \quad (3c)$$

Here, $f = 7.272\text{x}10^{-5}\ s^{-1}$ is the Coriolis parameter at 30° N; H = 3000 m is the basic-state depth;

$$h_s = h_0 \sin(4\pi x/D)[\sin(\pi y/D)]^2 \quad (3d)$$

is the terrain height; $D = 44d$ is the length of one side of the model domain; and $d = \Delta x = \Delta y$ = 300 km is the grid spacing. The maximum terrain height is set to h_0 = 250 m for the "true" model and to h_0 = 0 for the imperfect model in the OSSEs. The model domain is a square with periodic boundary conditions at x, y = 0 and D.

The "true" state is produced by integrating the "true" model (h_0 = 250 m) with the following geostrophically balanced conditions at the very beginning of the integration (48 hours before the starting time of the first data assimilation cycle):

$$h = 360[\sin(\pi y/D)]^2 + 120\sin(2\pi x/D)\sin(2\pi y/D),$$
$$u = -f^{-1}g\partial h/\partial y \text{ and } v = f^{-1}g\partial h/\partial x \text{ at } t = -48 \text{ hours.} \quad (4)$$

The model-produced "true" fields at t = 0 (after 48 hour integration to the starting time of the first assimilation cycle) are plotted in Fig. 1a. The "observations" are generated every 3 hours by adding random noises to the above model-produced "true" fields at sparsely and randomly selected grid points and the details will be described later.

3.2. Experiment Set-up

In all the OSSEs, the imperfect background state is produced by integrating the imperfect model (with h_0 = 0) from t = -48 hours [with the geostrophically balanced condition provided by (4)] to t = 0. In particular, the spatially averaged rms errors are 22.7 m, 1.50 and 2.64 m s^{-1} for the h-, u- and v-fields, respectively.

In each OSSE, the above imperfect initial state (at t = 0) is used to initialize the model and the model is integrated from t = 0 to $t = T + \tau/2$ to produce the 4D background field. By adding perturbations to the above imperfect initial state, the same model is integrated from t = 0 to $t = T + \tau/2$ to produce the perturbed 4D fields over the same time window in the first assimilation cycle. By using the background field and perturbed 4D fields, the incremental analysis is then performed (through the three steps described in section 2), and the analyzed field is used to update the background state at $t = T$ (the ending time of the first cycle). After the first assimilation cycle, the model is integrated from $t = T$ to $t = 2T + \tau/2$ for the next assimilation cycle, and so on so forth. In each experiment, the procedure goes through 10 cycles.

In all the OSSEs, the time length of the data assimilation cycle is set to T = 12 hours. However, the length of the analysis time window can vary as it is given by $\tau = (N_t - 1)\Delta\tau$, where N_t is the number of observation time levels covered by each analysis time window and $\Delta\tau$ = 3 hours is the observation time interval. The background fields are saved every 3 hours at the same time levels as the observations over each analysis time window. Each perturbed integration is initialized by superimposing a random field to the updated background state at the starting time of each cycle. The ensemble size is M = 150 and the truncation number for the expansion in (2) is p = 75 in OSSE-1 and OSSE-2 described below.

The OSSE-1 is designed to examine the robustness of the method, especially when the model is imperfect. For this purpose, two experiments are performed: one uses the perfect model (with h_0 = 250 m) and the other uses the imperfect mode (with h_0 = 0). Both experiments use five time levels of observations over each analysis time window, so N_t = 5 and the length of analysis time window is $\tau = (N_t - 1)\Delta\tau$ = 12 hours. Simulated observations are available in both the height and wind fields on a coarse grid and spaced every $3d$ = 900 km in the x- and y-directions. The observation errors are uncorrelated between different variables and different points in space and time. The observation error standard deviations are 12 m for h and 1.2 ms^{-1} for u and v.

OSSE-2 is designed to examine the robustness of the method with respect to incomplete observations. For this purpose, the method is applied to three types of

observations: type-1 is the same as in OSSE-1; type-2 is the same as type-1 but restricted to height only; and type-3 is the same as type-1 but restricted to wind only. With each type of observations, the 4D analysis is performed in each assimilation cycle in the same way as in OSSE-1.

OSSE-3 is designed to examine the sensitivities of the method to the truncation number p, observation error standard deviations, observation density and length of the analysis time window. It contains five experiments (Expts. 3.1-3.5).

4. RESULTS AND DISUSSIONS

4.1. Results of OSSE-1

The spatially averaged rms errors computed at each time level over the last analysis time window (that is, the 10th cycle) are used to evaluate the analysis accuracy. The results are listed in Table 1, where σ_h and $\sigma_{\mathbf{v}}$ denote the rms errors for the analyzed height h and wind $\mathbf{v} = (u, v)$ fields, respectively, As shown, the analyzed wind fields have nearly the same rms errors at the five different time levels. For the height fields, the differences at the five different time levels are not big too. This feature is seen in all the OSSEs, so we will only examine the results at the middle time level in the subsequent OSSEs.

Table 1. Spatially averaged rms errors, denoted by σ_h and $\sigma_{\mathbf{v}}$ for the height h and wind $\mathbf{v} = (u, v)$ fields, respectively, produced by En4DVar at the five time levels of the last (10th) cycle (from t = 108 to 120 hours) in OSSE-1.

Time level of the last cycle	$-2\Delta\tau$	$-\Delta\tau$	0	$+\Delta\tau$	$+2\Delta\tau$
Perfect model					
σ_h (m)	4.32	5.03	4.85	5.67	4.57
$\sigma_{\mathbf{v}}$ (m s^{-1})	0.58	0.57	0.57	0.57	0.57
Imperfect model					
σ_h (m)	7.45	8.65	8.19	9.67	8.55
$\sigma_{\mathbf{v}}$ (m s^{-1})	0.88	0.89	0.93	0.92	0.88

The resuslts in Table 1 also show that when the model is imperfect, the rms errors increase significantly (about 60% compared with the perfect-model results). The assimilation, however, still converges rapidly (within 10 cycles) as shown by the thick curves in Fig. 1 for imperfect-model case. In particular, when the model is imperfect, the analysis can still reduce the rms errors effectively in all the three (h, u and v) fields in each assimilation cycle. This leads to the convergence of the assimilation in spite of the vigorous growths of the forecast rms errors (thick curves) between every two adjacent analyses (from one cycle to the next cycle) caused by the model error. Thus, the method is quite robust and can work well for the imperfect model case, although the overall error reductions through the 10 cycles for the imperfect-model case are not as large as for the perfect-model case (Fig.1).

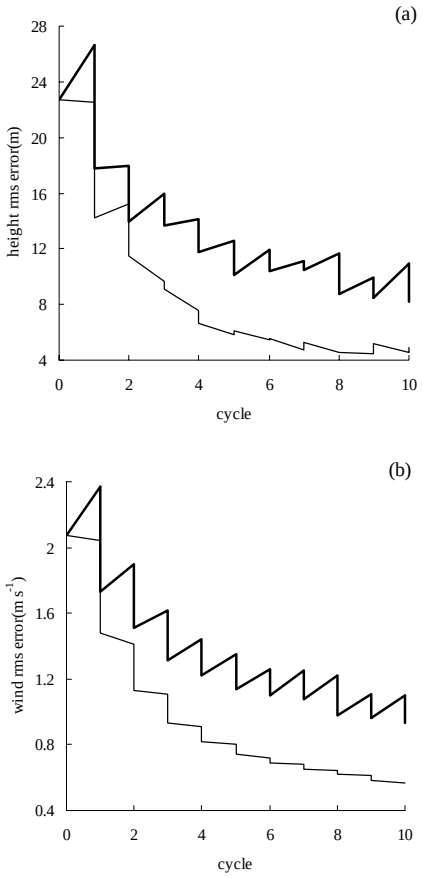

Fig. 1. Spatially averaged height rms errors (a) and wind rms errors (b) plotted as functions of assimilation time for the analyses obtained in OSSE-1 with the perfect model (thin curves) and imperfect model (thick curves). The drop of the error curve at each analysis time (every 12 hours) corresponds the error reduction made by the analysis.

4.2. Results of OSSE-2

The results of OSSE-2 are shown in the first column of Table 2 for the imperfect-model case. As shown, when observations are reduced from type-1 to type-2, the rms errors are increased from 8.19 to 10.47 m for the height analysis and from 0.93 to 1.36 m s^{-1} for the wind analysis at the time of the last update (t = 120 hours). Here, because the wind information is removed from the type-2 observations, the rms error is increased more (46.2%) in the wind analysis than that (27.8%) in the height analysis. Also as shown in Table 2 for the imperfect-model case, when observations are reduced from type-1 to type-3, the rms errors are increased from 8.19 to 9.82 m for the height analysis and 0.93 to 0.99 m s^{-1} for the wind analysis. Because the height information is removed from the type-3 observations, the rms error is increased more (19.9%) in the height analysis than that (6.45%) in the wind analysis. Note that the type-3 observations cover two component fields (for u and v) but the type-2 observations cover only one component field (for h). This explains why the rms

errors for the analysis with the type-3 observations are smaller than those with the type-2 observations.

When observations are reduced to type-2 (or type 3) and thus restricted to the height (or wind) field only, the En4DVar assimilation still converges rapidly (not shown but similar to that in Fig. 1). This implies that when the singular vectors are extracted from the ensemble of 4D difference fields sampled at multiple time levels (as described in section 2), the height-wind cross-correlation can be well represented in the background error covariance matrix constructed by the singular vectors not only for the perfect-model case but also for the imperfect-model case.

Note that an ensemble of 3D difference fields can be sampled at a single time level in each cycle. In this case, the analysis time window $= (N_t - 1)\Delta$ reduces to zero and the 4D analysis reduces to a 3D analysis. With the type-1 observations, this 3D analysis can be nearly as accurate as the 4D analysis. With the type-2 or type-3 observations, however, the 3D analysis becomes less or much less accurate than the 4D analysis, especially for the imperfect-model case. In the latter case, the 3D analysis even tends to diverge and thus cause the subsequent forecast to deviate rapidly from the true state (not shown). This implies that the background error covariance matrix is poorly constructed in the 3D analysis for the imperfect-model case. Because of this, the 3D analysis is not considered in this study.

4.3. Comparisons with EnKF and EnSRF

In this subsection, experiments are performed with two existing EnKF algorithms: (i) the efficient non-serial EnKF algorithm of Evensen (2003), and (ii) the serial algorithm of ensemble square root filter (EnSRF) of Whitaker and Hamill (2002). These two algorithms are denoted by EnKF-p and EnSRF-p, repectively, for the perfect-model case, but denoted by EnKF-ip0 (EnKF-ip1) and EnSRF-ip0 (or EnSRF-ip1), respectively, for the imperfect-model case with (or without) background error covariance inflation. The inflation factor is tuned to about 1.05 to optimize the analyses of EnKF-ip1 and EnSRF-ip1 for the imperfect-model case. In all these experiments, the ensemble size is set to be the same (M = 150) as in En4DVar.

Table 2. As in the last rows (imperfect-model case) of Table 1 but for the rms errors produced by En4DVar, En3DVar, EnSRF-ip0, EnSRF-ip1 and EnKF-ip1 at the time (t = 120 hours) of the last update in OSSE-2.

Method	En4D Var	EnSR F-ip0	EnSR F-ip1	EnKF-ip1
Type-1 obs (h and **v**)				
σ_h (m)	8.19	21.34	11.40	18.75
$\sigma_{\mathbf{v}}$ (m s^{-1})	0.93	1.98	1.52	2.36
Type-2 obs (h only)				
σ_h (m)	10.47	17.73	10.50	16.93
$\sigma_{\mathbf{v}}$ (m s^{-1})	1.36	1.79	1.71	3.21
Type-3 obs (**v** only)				
σ_h (m)	9.82	25.09	14.40	51.08
$\sigma_{\mathbf{v}}$ (m s^{-1})	0.99	1.79	1.40	2.44

To filter spurious long-range correlation caused by finite ensemble sizes, compactly supported smooth isotropic correlation functions (Gaspari and Cohn 1999) have been used to localize the EnKF computed covariance (Houtekamer and Mitchell 2001; Whitaker and Hamill 2002). Such a localization is convenient for the EnSRF but not for the efficient non-serial EnKF algorithm of Evensen (2003). Thus, the background error covariance is not localized in EnKF-p, EnKF-ip0 and EnKF-ip1. The covariance localization radius is tuned to 3d (= 3Δx = 3Δy = 900 km) to optimize the analyses of EnSRF-p, EnSRF-ip0 and EnSRF-ip1.

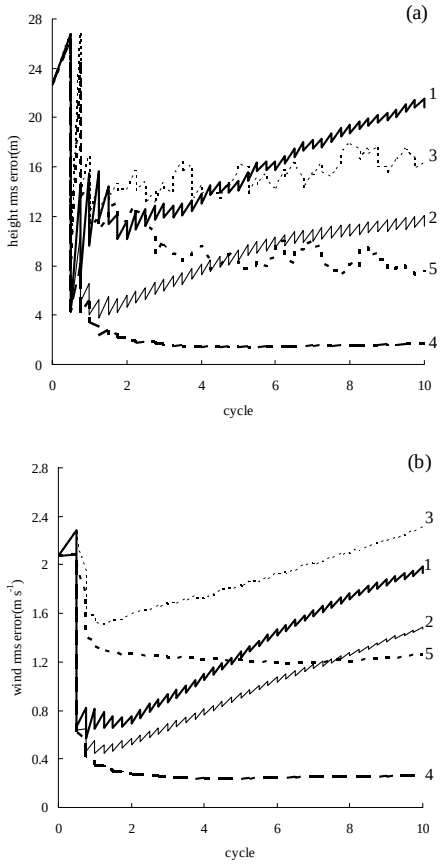

Fig. 2. Height rms errors (a) and wind rms errors (b) plotted as functions of assimilation time for the analyses performed with type-1 observations by different algorithms (with six different settings): EnSRF-ip0 (curve-1 for the imperfect-model case without inflation), EnSRF-ip1 (curve-2 for the imperfect-model case with inflation), EnKF-ip1 (curve-3 for the imperfect-model case with inflation), EnSRF-p (curve-4 for the perfect-model case), and EnKF-p (curve-5 for the perfect model case). The drop at each analysis time (every 3 hours) corresponds the error reduction made by the analysis.

The above algorithms (with six different settings) are tested with the same type-1 observations as in OSSE-1. As the observations are available every 3 hours, the assimilation is cycled here every 3 hour. The rms errors are plotted in Fig. 2. As shown, for the perfect-model case, EnSRF-p (curve-4) performs better but EnKF-p

Table 3. As in Table 2 but for rms errors produced by En4DVar with different settings of the truncation number p (Expts. 3.1 and 3.2), observation errors (Expt. 3.3), observation density (Expt. 3.4), and analysis time window (Expt. 3.5) in OSSE-3. The control experiment (first column) is the same as that in the first column of Table 2.

Expt.		Control (p = 75)	#3.1 p = 50	#3.2 p = 100	#3.3 obs error ×1.5	#3.4 obs spacing = 5d	#3.5 window = 6 h
Type-1 obs (h and **v)**	$_h$ (m)	8.19	8.96	6.60	9.00	12.28	8.28
	$_{\mathbf{v}}$ (m s^{-1})	0.93	1.19	0.85	1.03	1.23	0.92
Type-2 obs (h only)	$_h$ (m)	10.47	12.37	9.51	11.66	16.24	9.66
	$_{\mathbf{v}}$ (m s^{-1})	1.36	1.61	1.27	1.50	1.66	1.35

(curve-5) performs worse than En4DVar (thin curves in Fig. 1). For the imperfect-model case, the algorithms (with four different settings) all perform worse than En4DVar (thick curves in Fig. 1). Among the four, EnKF-ip0 performs worst (not shown) and EnSRF-ip1 performs best. With the background error covariance properly inflated, the rms errors become smaller in EnSRF-ip1 than in EnSRF-ip0, but the errors still increase with assimilation time at nearly the same rate as in EnSRF-ip0 (compare curve-2 with curve-1 in Fig. 2). Thus, even for the best performer (that is, EnSRF-ip1), the assimilation still does not converge (see curve-2 in Fig. 2).

The EnKF and EnSRF algorithms (with six different settings) are also tested with the type-2 and type-3 observations (as in OSSE-2). The results exhibit basically the same features as obtained above with the type-1 observations, except that the rms errors become even larger and increase more rapidly with the assimilation cycle for the imperfect-model case (not shown). Thus, En4DVar still performs substantially better than EnSRF and EnKF for the imperfect-model case.

The rms errors for the analyses produced by EnSRF-ip0, EnSRF-ip1 and EnKF-ip1 are listed in the last three columns of Table 2 in comparison with those produced by En4DVar (first column) in OSSE-2. The listed results show again that En4DVar performs better than EnKF and EnSRF for the imperfect-model case. Note that the rms errors are listed in Table 2 for the analyses at t = 120 hours, while the errors keep increasing with time for the analyses produced by EnSRF-ip0, EnSRF-ip1 and EnKF-ip1. Thus, En4DVar is more robust than EnSRF and EnKF for the imperfect-model case.

EnKF or EnSRF computes the background mean and covariance approximately from an ensemble of model solutions (3D fields) at the analysis time. The computed back background mean and covariance can become poor or even invalid representations of the true mean and covariance when the model contains significant errors including biases. The situation can become increasingly worse as the ensemble is cycled but not

adequately corrected by the analysis in each cycle. This explains why the assimilation does not converge in EnSRF-ip1 and EnKF-ip1 even though the covariance is optimally inflated (see curve-2 and curve-3 in Fig. 2).

4.4. Results of OSSE-3 and Sensitivities of En4DVar

In OSSE-3, five experiments (Expts. 3.1-3.5) are designed to test the sensitivities of En4DVar to the truncation number p, observation error standard deviations, observation density and length of analysis time window. The control experiment is the same as in OSSE-2 for the imperfect-model case. The truncation number p is decreased from p = 75 to 50 (with $\sum_{k=1}^{p} E_k$ decreased from 0.956 to 0.922) in Expt. 3.1 but p is increased to 100 (with $\sum_{k=1}^{p} E_k$ increased to 0.976) in Expt. 3.2. The observation error standard deviations (12 m for h and 1.2 m s^{-1} for u and v) are increased by 50% in Expt. 3.3. The observation spacing is increased from every 3d (= 900 km) to every 5d = (1500 km) in the x- and y-directions in Expt. 3.4. The analysis time window is decreased from 12 hours to 6 hours in Expt. 3.5.

The results for the control experiment are listed in the first column of Table 3 and this column is identical to the first column of Table 2. The results listed for Expts. 3.1 and 3.2 in Table 3 indicate that the analysis accuracy is not sensitive moderately to the truncation number as $p \geq 75$ but becomes moderately sensitive as p decreases below 75. Although the analysis can be improved significantly as p is increased from 75 to 100,

The results of Expts. 3.3 and 3.4 indicate that the analysis accuracy is not very sensitive to observation error but relatively sensitive to observation density. From the results of Expt. 3.5, we can see that the analysis accuracy does not change much when the analysis time window is reduced from 12 to 6 hours. For the perfect-modal case, all the rms errors listed in Table 3 are reduced and so are their reflected sensitivities. The qualitative sensitivity features obtained above for the imperfect-modal case, however, remain valid for the perfect-modal case.

5. SUMMARY AND CONCLUSIONS

In En4DVar method proposed in this paper, the incremental analysis in each assimilation cycle is produced by fitting a linear combination of the leading singular vectors extracted from an ensemble of 4D perturbation solutions to 4D innovation data (observation minus background). In the costfunction used for the fitting, the background error covariance

matrix is constructed implicitly by the perturbation solutions (through their representative singular vectors). The robustness and potential merits of the method are demonstrated by three sets of observing system simulation experiments performed with a two-dimensional shallow water equation model. The main results are summarized as follows:

(i) The method is robust even when the model contains a significant bias error.

(ii) The method is also robust with respect to incomplete observations (restricted to either height only or wind only).

(iii) The method is not very sensitive to the SVD truncation as long as the truncation number is not small (with $\sum_{k=1}^{p} E_k$ ensured to be larger than 0.95). The method is moderately sensitive to observation density but not sensitive to the reduction of the analysis time window (from 12 to 6 hours) even for the imperfect-model case.

Because only the mean (rather than the entire ensemble of perturbation solutions) is updated by the analysis into the next cycle, the proposed En4DVar is less accurate than the ensemble square root filter (EnSRF) of Whitaker and Hamill (2002) for the perfect-model case although it is more accurate than EnKF without localization (see Fig. 2). For the imperfect-model case, the proposed method still converges rapidly (see Fig. 1) but EnKF and EnSRF do not converge (see Fig. 2). The results suggest that if the model is imperfect and contains significant biases, then continuously using the same updated ensemble may accumulate of model biases and thus may not be a good strategy. The advantages of 4D analyses over 3D analyses are also evidenced by deteriorated performances (not shown in this paper) caused by degrading the 4D analyses in En4DVar into 3D analyses (as discussed at the end of section 4.2).

The results obtained in this paper are encouraging. In particular, the proposed En4DVar is shown to be able to alleviate some problems caused by model errors (especially biases) while these problems can be notoriously difficult for the advanced techniques. This may imply that the subspace spanned by the leading singular vectors can cover the dominant uncertainties in the model solutions caused by errors not only in the initial conditions but also in model equations. As the subspace spanned by the leading singular vectors is compact and yet can still contain the attractors of the modeled atmospheric dynamics in the phase space, the least-squares fitting used in the method can be very efficient and well determined. As explained earlier, updating only the mean but not the entire ensemble of perturbation solutions at each analysis step of En4DVar can make the method less vulnerable to model errors, but it may also severely limit the accuracy of the method as the model becomes increasingly accurate or model error statistics can be adequately estimated. This limitation may be reduced if the ensemble perturbation solutions are properly rescaled at the end of each assimilation cycle and partially re-used in the next cycle in a way somewhat similar to the breeding method (Toth and Kalnay 1997). Further improvements in this direction are under investigation.

Acknowledgments. This work was supported by the Grant 40575049 from National Science Foundation of China to Lanzhou University and by the ONR Grants N000140310822 and N000140410312 to University of Oklahoma. Funding was also provided to CIMMS by NOAA/Office of Oceanic and Atmospheric Research under NOAA-University of Oklahoma Cooperative Agreement #NA17RJ1227, U.S. Department of Commerce.

REFERENCES

Evensen, G, 2003: The ensemble Kalman filter: Theoretical formulation and practical implementation. *Ocean Dynamics*, **53**, 343-367.

Hamill, T. M., and C. Snyder 2000: A hybrid ensemble Kalman filter-3D variational analysis scheme. *Mon. Wea. Rev*, **128**, 2905–2919.

Houtekamer, P. L, and A. L. Mitchel, 1998: Data assimilation using ensemble Kalman filter technique, *Mon. Wea..Rev.* **126**, 796-811.

Lorenc, A， 2003：The potential of the ensemble Kalman . lter for NWP—a comparison with 4D-Var. *Q. J. R. Meteorol. Soc.*, **129,** 3183–3203.

Whitaker, J. S. and Hamill, T. M. 2002. Ensemble data assimilation without perturbed observations. *Mon. Wea. Rev.* **130**, 1913-1924.

Zupanski, M., 2005: Maximum likelihood Ensemble filter: theoretical aspects. *Mon. Wea. Rev.*, **133**, 1710–1726.